Chemistry & Biology
Article

Structure and Function of the Glycopeptide *N*-methyltransferase MtfA, a Tool for the Biosynthesis of Modified Glycopeptide Antibiotics

Rong Shi,[1] Sherry S. Lamb,[2] Bijan Zakeri,[2] Ariane Proteau,[1] Qizhi Cui,[3] Traian Sulea,[3] Allan Matte,[3] Gerard D. Wright,[2] and Miroslaw Cygler[1,3,*]
[1]Department of Biochemistry, McGill University, 3655 Promenade Sir William Osler, Montréal, QC H3G 1Y6, Canada
[2]MG DeGroote Institute for Infectious Disease Research, Department of Biochemistry and Biomedical Sciences, McMaster University, 1200 Main Street West, Hamilton, ON L8N 3Z5, Canada
[3]Biotechnology Research Institute, National Research Council, 6100 Royalmount Avenue, Montréal, QC H4P 2R2, Canada
*Correspondence: mirek@bri.nrc.ca
DOI 10.1016/j.chembiol.2009.02.007

SUMMARY

There is a considerable interest in the modification of existing antibiotics to generate new antimicrobials. Glycopeptide antibiotics (GPAs) are effective against serious Gram-positive bacterial pathogens including methicillin-resistant *Staphylococcus aureus*. However, resistance to these antibiotics is becoming a serious problem requiring new strategies. We show that the *Amycolatopsis orientalis* (*S*)-adenosyl-*L*-methionine-dependent methyltransferase MtfA, from the vancomycin-class GPA chloroeremomycin biosynthetic pathway, catalyzes in vivo and in vitro methyl transfer to generate methylated GPA derivatives of the teicoplanin class. The crystal structure of MtfA complexed with (*S*)-adenosyl-*L*-methionine, (*S*)-adenosylhomocysteine, or sinefungin inhibitor, coupled with mutagenesis, identified His228 as a likely general base required for methyl transfer to the N terminus of the glycopeptide. Computational docking and molecular dynamics simulations were used to model binding of demethyl-vancomycin aglycone to MtfA. These results demonstrate its utility as a tool for engineering methylated analogs of GPAs.

INTRODUCTION

In recent years, the increasing occurrence of bacterial resistance to antibiotics has become a serious threat to human health. Glycopeptide antibiotics (GPAs) such as vancomycin and teicoplanin are important drugs for the treatment of nosocomial and community acquired infections caused by multidrug-resistant Gram-positive pathogens. Vancomycin was considered a drug of last resort often reserved for the treatment of systemic infections caused by methicillin-resistant *Staphylococcus aureus* (Kahne et al., 2005). However, the increasing prevalence of infections due to vancomycin-resistant *S. aureus* (VRSA and VISA) and *Enterococci* has been observed with the increase in vancomycin use, indicating that the utility of this antibiotic is seriously threatened (Murray, 2000; Van Bambeke et al., 2004). The introduction of anti-Gram-positive agents such as quinupristin/dalfopristin, daptomycin, and linezolid in recent years has improved the situation somewhat, but these are already facing the emergence of resistance (Van Bambeke et al., 2004). This serious and growing threat underscores the need for novel antibiotics, including diverse semisynthetic derivatives of GPAs, active against resistant bacterial strains.

GPAs are structurally complex natural products consisting of a heptapeptide skeleton that is assembled via nonribosomal peptide synthesis. GPAs can be divided into two major classes, vancomycin and teicoplanin, based on the chemical structure of their peptide cores (Figure 1). The structural diversity of natural GPAs is mainly derived from enzymatic modifications of the peptide that can include aryl crosslinking, glycosylation, methylation, hydroxylation, halogenation, acylation, and sulfation (Kahne et al., 2005). These modifications at various sites on the heptapeptide core can be utilized to produce GPA analogs displaying improved properties and in vivo efficacy. Previous reports have shown that even modest structural modifications of vancomycin can overcome resistance (Rodriguez et al., 1998). A successful strategy is the semisynthetic modification of these compounds, which has already led to three second-generation GPAs (oritavancin, telavancin, and dalbavancin) that are in late-stage clinical trials (Attwood and LaPlante, 2007; Poulakou and Giamarellou, 2008; Billeter et al., 2008). These successes have created considerable interest in expanding the structural diversity of GPAs and prompted closer examination of the biosynthetic logic for the assembly of this class of antibiotics. Gene clusters involved in the biosynthesis of the GPAs balhimycin, chloroeremomycin, A40926, A47934, and teicoplanin have been identified (Donadio et al., 2005). The transferases from these GPA biosynthetic pathways constitute a promising toolbox for combinatorial manipulation to generate new semisynthetic antibiotics. For example, some glycosyltransferases from the vancomycin and chloroeremomycin pathways and the sulfotransferase StaL from the A47934 pathway can effectively utilize nonnatural substrates to generate new compounds (Losey et al., 2002; Lamb et al., 2006). Furthermore, modifying the specificity of these transferases by protein engineering could be exploited to increase the diversity of products. The structure-function studies of several glycosyltransferases (Mulichak et al., 2003, 2004) and a sulfotransferase (Shi et al., 2007) have been reported. However, little is known about the structure, the determinants of recognition, or the selectivity for any methyltransferase in these pathways.

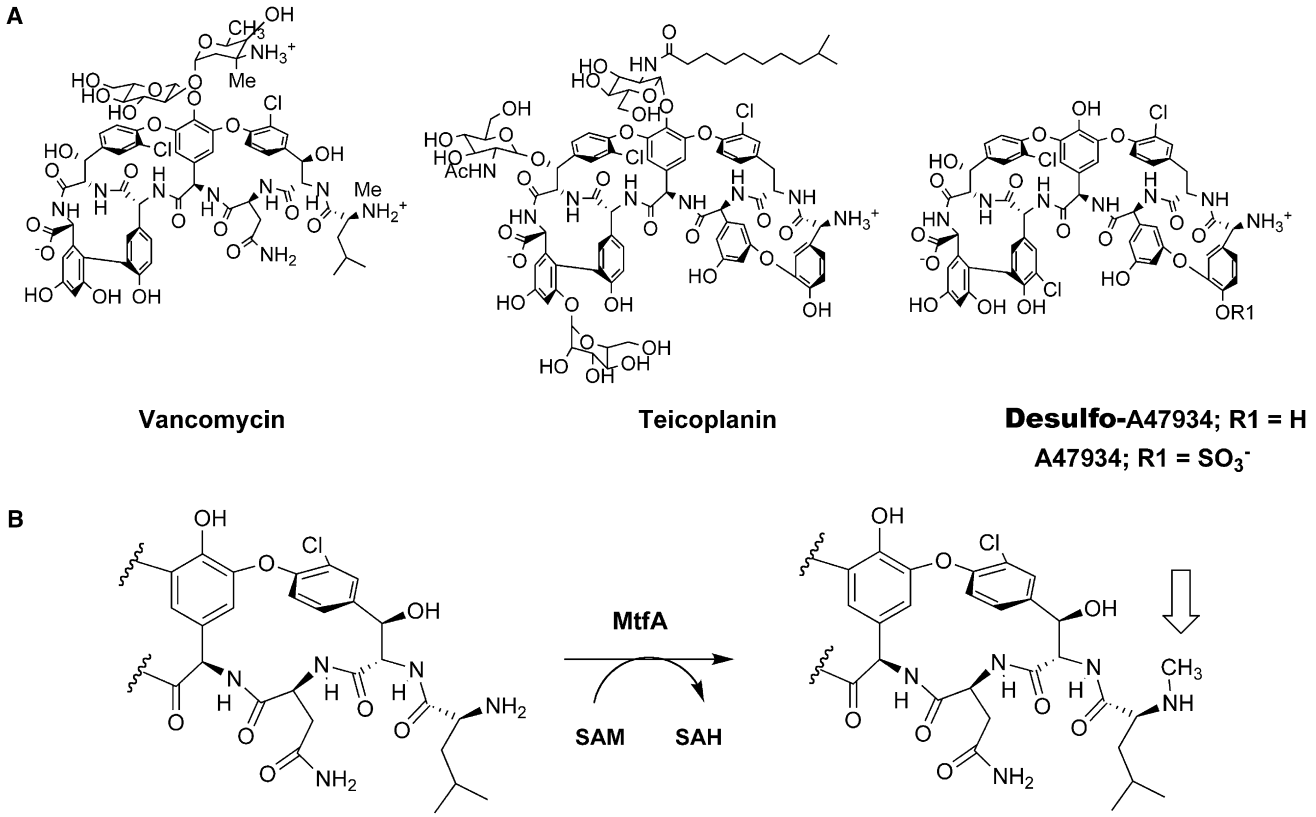

Figure 1. GPAs

(A) Vancomycin, teicoplanin, and A47934 GPA peptide scaffolds.

(B) The reaction catalyzed by MtfA with the site of methylation indicated by an arrow.

MtfA is an (*S*)-adenosyl-*L*-methionine (SAM)-dependent *N*-methyltransferase (MTase) from the GPA chloroeremomycin biosynthetic cluster in *Amycolatopsis orientalis* (van Wageningen et al., 1998). The *N*-methylation catalyzed by MtfA is a late step reaction in chloroeremomycin biosynthesis, taking place after the oxidative crosslinking of the heptapeptide but before the glycosylation (O'Brien et al., 2000). This suggests that MtfA could be a good addition to the arsenal of promiscuous enzymes for generating antibiotic diversity. MtfA has two orthologs, a putative MTase from *Amycolatopsis balhimycina* involved in balhimycin biosynthesis (Recktenwald et al., 2002) and that from *Nonomuraea* species ATCC 39727 involved in the biosynthesis of the GPA A40926 (Sosio et al., 2003). Very recently, studies on a new glycopeptide synthesis gene cluster found in an environment DNA megalibrary have identified another two new methyltransferases involved in the biosynthesis of previously unknown glycopeptides (Banik and Brady, 2008). These enzymes share ~55%–76% amino acid sequence identity and have a strictly conserved SAM-binding motif, (G(A)xGxG), that is found among other SAM-dependent MTases (Schubert et al., 2003). Together, they represent a unique group of MTases that are involved in the biosynthesis of GPAs of both the vancomycin and teicoplanin structural classes.

SAM-dependent MTases are involved in a variety of physiological functions, including biosynthesis, signal transduction, and DNA or RNA modification and previous studies have elucidated many crystal structures for these enzymes (Schubert et al., 2003). MTases exhibit great diversity in their tertiary structures and in their substrate-binding sites, as well as in the conformations of bound SAM/(*S*)-adenosylhomocysteine (SAH). Although these MTases have been classified into five structural classes (I–V) (Schubert et al., 2003), the sequence identities among the MTases are low, even in the same structural class. Therefore, based on the primary sequence it is hard to predict their cognate 3D structure, the binding mode of the cofactor, and the substrate specificity for a given MTase.

Here, we report the application of MtfA in the in vivo and in vitro synthesis of methylated GPA derivatives. To better understand the specificity of MtfA, we have determined its crystal structure as well as the structures of MtfA complexes with SAM, SAH, and the SAM analog sinefungin, a potent MTase inhibitor (Pugh et al., 1978). This is the first crystal structure of a methyltransferase involved in GPA biosynthesis and the first example of the expansion of GPA chemical diversity by *N*-methylation of a teicoplanin scaffold antibiotic with a vancomycin scaffold methyltransferase.

RESULTS AND DISCUSSION

MtfA Methylates Teicoplanin Scaffold GPAs Generating New Natural Products

The *mtfA* gene was integrated as a single copy into the genome of the desulfo-A47934 producer *Streptomyces toyocaensis*

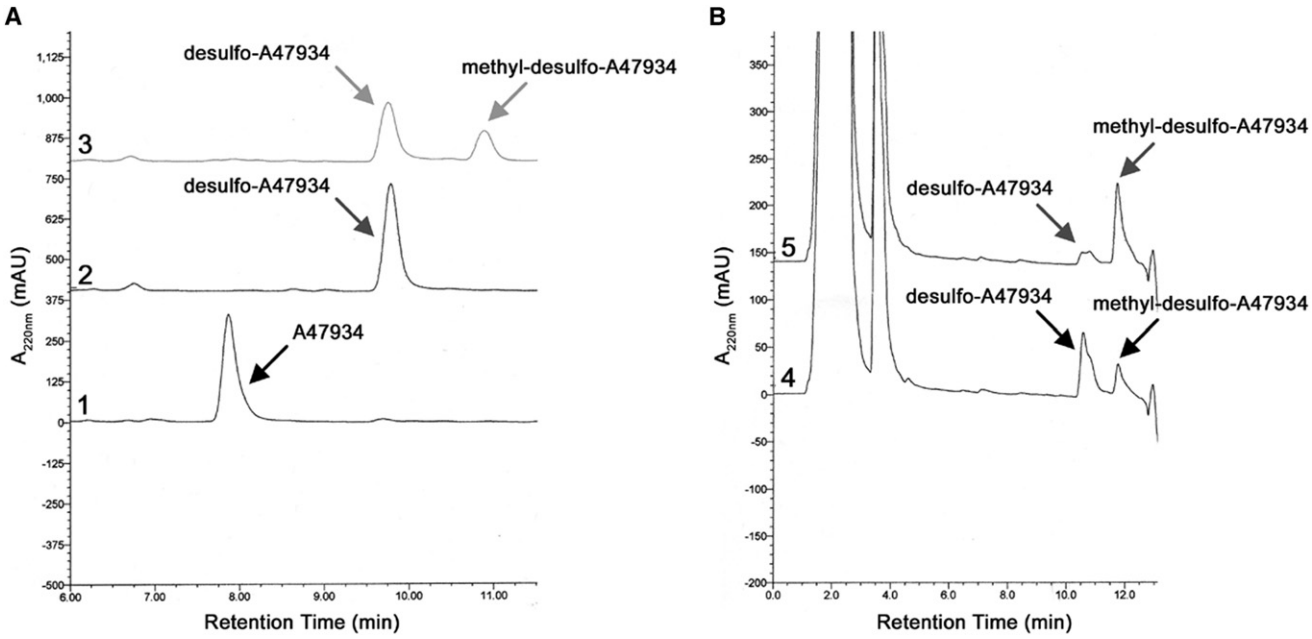

Figure 2. MtfA Methylates Teicoplanin Scaffold Antibiotics

(A) RP-HPLC analysis of cell-free extracts from wild-type *S. toyocaensis* (Trace 1), *S. toyocaensis ΔstaL*::*aac(3)IV* (Trace 2), and *S. toyocaensis ΔstaL*::*aac(3)IV* ΦC31::*mtfA*/pIJ8600 (Trace 3) showing the in vivo methylation of desulfo-A47934 (R_t = 9.8 min) to methyl-desulfo-A47934 (R_t = 10.9 min).

(B) RP-HPLC analysis of the cell-free extract from *S. toyocaensis ΔstaL*::*aac(3)IV* ΦC31::*mtfA*/pIJ8600 in a control reaction with no His_6-MtfA added (Trace 4) and the same extract after incubation with purified His_6-MtfA and SAM (Trace 5) resulting in the in vitro methylation of desulfo-A47934 (R_t = 10.6 min) to generate more methyl-desulfo-A47934 product (R_t = 11.7 min).

ΔstaL::*aac(3)IV*. Fermentation by this dual engineered organism resulted in the in vivo production of methyl-desulfo-A47934 (Figure 2A and Table 1). The methylated compound was estimated to be 25% of the total GPA produced by this strain. Addition of His_6-MtfA and SAM to the crude extract readily converted the antibiotic to the methylated version (Figure 2B). MtfA therefore can be used in vivo and in vitro to generate methylated GPAs with noncognate peptide scaffolds.

Recombinant His_6-MtfA was incubated with purified A47934 and its nonsulfated analog desulfo-A47934 (Lamb et al., 2006). Unlike chloroeremomycin, which has the vancomycin peptide scaffold, A47934 has the teicoplanin peptide scaffold (Figure 1) containing only aromatic amino acids. His_6-MtfA did not recognize A47934 as a substrate, but did methylate desulfo-A47934 in a SAM-dependent manner, generating methyl-desulfo-A47934 (Table 1). Similarly, the lipoglycopeptide teicoplanin could also be methylated (Table 1), demonstrating that MTases can be used to generate a range of methylated GPA derivatives.

Table 1. LC/ESI-MS Data for Methyl- and Desmethyl-GPAs

Antibiotic[a]	Predicted MW (Da)	Observed *m/z*
		1232.2 $[M-H]^-$
Desulfo-A47934	1233.4	1233.1 $[M+H]^+$
		1246.3 $[M-H]^-$
Methyl-desulfo-A47934	1247.4	1247.2 $[M+H]^+$
A47934	1313.4	1312.6 $[M-H]^-$
Teicoplanin	1879.7	939.4 $[M-H]^{2-}$
Methyl-teicoplanin	1893.7	946.0 $[M-H]^{2-}$

[a] The *m/z* value of 1327.5 for methyl-A47934 was not observed in the fermentation broth of *S. toyocaensis* ΦC31::*mtfA*/pIJ8600 nor in the in vitro reaction with purified His_6-MtfA using A47934 as a substrate. However, the *m/z* value corresponding to A47934 was observed in these samples.

Crystal Structure of MtfA

To understand MtfA at the molecular level and to visualize its substrate-binding site, we have crystallized this protein and determined its 3D structure. Size-exclusion chromatography and dynamic light scattering showed that the apparent molecular mass of MtfA is 66 kDa and 58 kDa, respectively, clearly indicating the presence of dimers in solution. In the crystal there are two MtfA molecules in the asymmetric unit also forming a dimer, which we conclude represents the biological unit.

MtfA has an unusual shape, with two wing-like structures extending from the main body of the protein (Figure 3A). There are 9 α helices and 11 β strands in total. The bulk of the protein consisting of residues 47–173 and 234–280 is folded into an extended Rossmann fold domain. This domain is made of a central, parallel seven-stranded β sheet, β4-β3-β2-β5-β6-β11-β10, where all except β11 are parallel with one another, with four helices (α2–α5) on one side of the sheet and three (α6, α7, and α9) on the other side. The insertion formed by residues 174–233 generates two long, two-stranded β sheets extending from the top of the Rossmann fold domain in both directions forming "wings." The first ~45 N-terminal residues interact with one of the wings (Figure 3A).

The fold of the main domain classifies MtfA as a class I MTase (Schubert et al., 2003). However, the sequence identity between this domain of MtfA and other proteins is low, with the highest

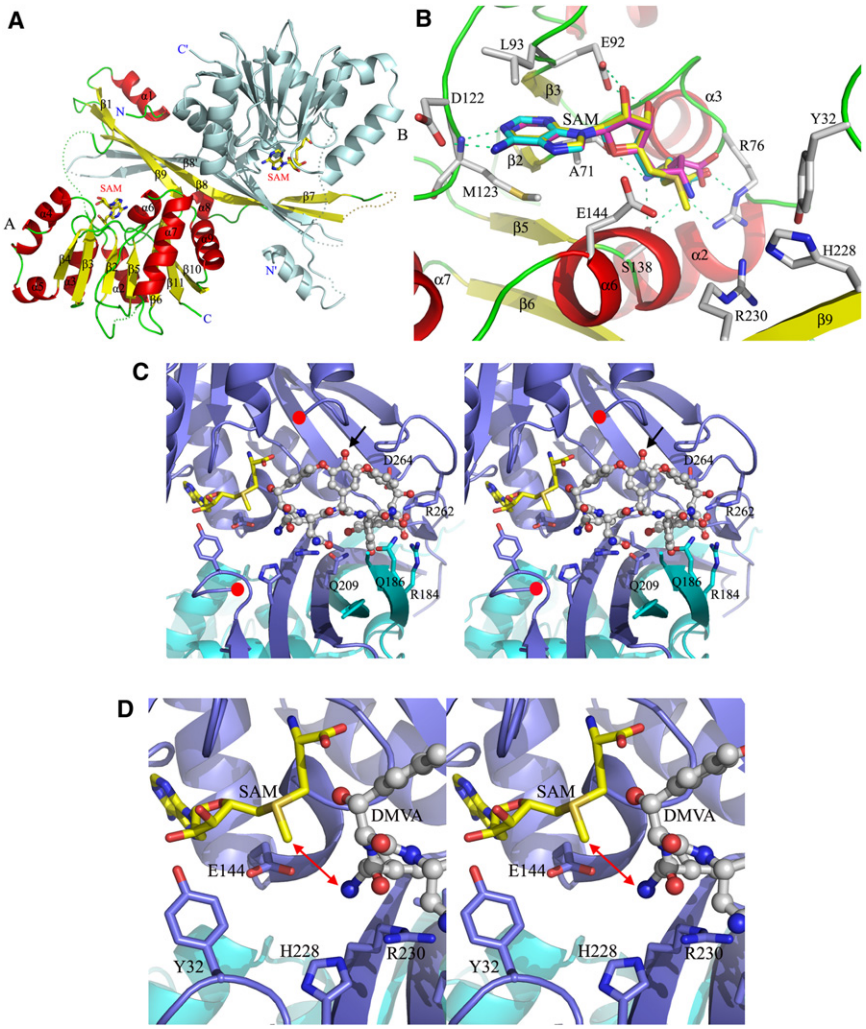

Figure 3. Structure of MtfA

(A) Dimerization of MtfA. In monomer A, the helices are red, strands yellow, and loops green. Monomer B is colored cyan. The SAM molecule is shown as sticks. Dotted lines show the missing loops.

(B) Cofactor-binding pocket in MtfA with superposed SAM (carbons colored yellow), SAH (cyan), and sinefungin (magenta). The H bonds between SAM and MtfA are shown.

(C) The ball-and-sticks model of the DMVA substrate binding in the ternary complex with MtfA and SAM. Monomer A is blue and B is cyan. Red dots indicate the ends of the Ala36-Asp48 disordered loop. The known *O*-glycosylation site of vancomycin is indicated by an arrow.

(D) Close-up of the catalytic center showing the nucleophilic N1 nitrogen atom of DMVA, the electrophilic *S*-methyl carbon atom of SAM, and the mutated residues Tyr32, Glu144, His228, and Arg230. The reactive atom pair is indicated with a red double arrow. The figure was prepared using PyMol (www.pymol.org).

amino acid sequence identity to a MTase of unknown function from *Clostridium acetobutylicum* (17%; PDB code 1Y8C). Other structurally related proteins include the pyocyanin biosynthetic protein PhzM from *Pseudomonas aeruginosa* (PDB code 2IP2) and the sugar *N*,*N*-dimethyltransferase from *Streptomyces venezuelae* (PDB code 3BXO), chalcone *O*-methyltransferase from *Medicago sativa* (Alfalfa) (PDB code 1FP1), and glycine *N*-methyltransferase from rat liver (PDB code 1XVA).

Novel Dimerization Motif

The dimerization motif found in MtfA (Figure 3A; see Figure S1 available online) is unique to this MTase and has not been observed in any other MTase for which structures have been determined. The monomers associate through the pairing of the two-stranded β sheet wings extending from the central, Rossmann fold domain to form a four-stranded antiparallel β sheet. The two central β strands forming the zipper are made from residues 193–215 (strand β8) from each subunit (Figure 3A and Figure S1). Both hydrophilic and hydrophobic interactions contribute to the stabilization of the dimer, with over 20 hydrogen bonds in the dimerization interface, contributed mainly by main chain atoms. The total surface area buried upon dimer formation is ~3550 Å^2 per monomer, accounting for ~30% of the total monomer surface area. This mode of dimerization creates a deep canyon between the cofactor-binding domain and four β strands (β8 and β9 from subunit A and β7′ and β8′ from subunit B), with the SAM cofactor-binding site located at the bottom of the canyon (Figures 3B and 3C). The large size of this canyon matches that required for binding a GPA and the contribution from both subunits indicates that dimerization is essential for MtfA activity. This dimerization mode is likely common to other MTases involved in GPA biosynthesis from *A. balhimycina* and *Nonomuraea* species ATCC 39727 based on sequence similarity to MtfA, not only within the Rossmann fold domain but also within the wings (Figure S2).

The SAM/SAH/Sinefungin Binding Site

The SAM cofactor is bound near the β2/α3 loop containing the consensus sequence E^{69}xAxGxG^{75} (Figure 3B), the hallmark SAM-binding motif of Rossmann fold SAM-dependent MTases, and corresponds well to the location of the cofactor in other SAM-dependent MTases (Schubert et al., 2003). SAM forms several hydrogen bonds and hydrophobic interactions (Figure 3B). The adenine ring is sandwiched between Leu93 on one side and Met123 and Ala71 on the other side, with the adenine ring participating in two hydrogen bonds: N1…HN^{Met123} and N6…OD1^{Asp122}. The ribose hydroxyl groups are hydrogen bonded to the side chain of Glu92 and the O5 atom packs against Ala71. The methionine *S*-methyl group contacts Gly140 and Ser141, the carboxyl group forms a salt bridge with Arg76 and a hydrogen bond to OG^{Ser138}, and the amide group is H bonded to the same OG^{Ser38} and to the O^{Ala71}.

Table 2. Activity of MtfA Wild-Type and Mutant Enzymes

Enzyme	Activity (%)[a]
No Enzyme	0.0
MtfA wild-type	50.6 ± 3.4
MtfA Y32F	11.6 ± 1.5
MtfA E144A	9.3 ± 2.1
MtfA H228A	0.0
MtfA R230A	15.1 ± 4.4

[a] Enzymatic reactions were performed under initial rate conditions in triplicate with desulfo-A47934 as a substrate and analyzed by RP-HPLC. Reaction conditions were as follows: 50 mM HEPES buffer (pH 7.5), 0.5 mM SAM, 50 μM desulfo-A47934, and 3 μg of enzyme in a 50 μL reaction incubated for 24 hr at 30°C; subsequently, the reaction was stopped by the addition of 1 vol of 1% (v/v) trifluoroacetic acid. Activity is reported as the percent conversion with standard deviation.

The structure of MtfA-SAH, the demethylated product of SAM, shows that, as expected, SAH binds in the same location as SAM and forms similar interactions with the enzyme. We have also determined the crystal structure of MtfA complexed with the MTase inhibitor sinefungin. The adenosine moiety of sinefungin binds in the same manner as that of SAM/SAH; however, its ornithine moiety is slightly rotated relative to the amino acid moieties of SAM/SAH and its carboxyl and amide groups form H bonds through bridging water molecules, except for one direct bond to Arg78 (Figure 3B).

Characterization of Active Site Mutants

Based on the MtfA-SAM crystal structure and residue types previously identified as participating in deprotonation of the N atom of the substrate (Schubert et al., 2003), we selected four residues, Tyr32, Glu144, Arg230 (located less than 6 Å from the methyl group of SAM), and His228 (8.5 Å away) for site-directed mutagenesis. These mutants were expressed, purified, and their specific activity measured using desulfo-A47934 as a substrate. Tyr32 is the only tyrosine in the vicinity of SAM but the Y32F mutation reduces activity only ~5-fold (Table 2). Similarly, the mutations E144A and R230A reduced activity only ~3- to 5-fold. Therefore, these residues likely play a role in substrate or cofactor binding but are not essential for catalysis. However, the H228A mutation abolished methylation of desulfo-A47934, although it was folded similarly to the wild-type protein based on its circular dichroism spectrum and behaved as a dimer in size exclusion chromatography (data not shown). We suggest that His228 is the most likely candidate to act as a general base during catalysis.

Modeling of Antibiotic Binding

Efforts to obtain the crystal structure of MtfA with bound desulfo-A47934 or vancomycin aglycone, the product of MtfA acting on demethyl-vancomycin aglycone (DMVA), have so far been unsuccessful. We have used computational docking and molecular dynamics (MD) simulation to derive a model of the MtfA-SAM-DMVA complex. During the calculations, the reactive N1 nucleophilic nitrogen atom of DMVA was restrained to be in proximity to the His228 imidazole and to the reactive *S*-methyl carbon atom of SAM. The average simulated structure of the ternary complex, energy-minimized without restraints, positions the DMVA substrate in a well-shaped pocket formed by both subunits of the dimer (Figures 3C and 3D). DMVA forms seven hydrogen bonds to the side chains of Gln209, Arg262, and Asp264 from the A subunit and Arg184 and Gln186 from the B subunit of MtfA. The side chains of residues 1 and 7 of DMVA insert deeply into the substrate-binding cleft contacting residues Gly140, Ala172, and Leu232 of the A subunit. The *O*-glycosylation site of vancomycin at residue 4 is solvent exposed (Figure 3C), consistent with the observation that demethyl-vancomycin is a substrate of MtfA (O'Brien et al., 2000). Teicoplanin, another MtfA substrate (Table 1), when positioned based on the model of DMVA, would have its glycosylation sites at residues 4 and 6 exposed, while the mannose sugar at residue 7 would be accommodated in a cavity between MtfA and the aglycone scaffold. The loop Ala36-Asp48, disordered in the present structures, would form a bridge directly over the DMVA docking site, likely interacting with the substrate (Figure 3C). The DMVA model also provides a plausible answer as to why A47934 is not a substrate for MtfA, while desulfo-A47934 is methylated by this enzyme. Superimposing the backbone of A47934 on the backbone of vancomycin shows that the sulfate group would be located on the side of the substrate facing the protein and may hinder its productive binding to the enzyme.

Proposed Mechanism of Catalysis

Most enzyme-catalyzed methyl transfer reactions proceed by one of two strategies, either donation of a methyl group from methyl-tetrahydrofolate or through donation from SAM (Schubert et al., 2003). The transfer of the methyl moiety from SAM to the acceptor occurs with concomitant formation of SAH. It has been shown that MTases can utilize different residues as a general base, including tyrosine (lysine *N*-methyltransferase [Guo and Guo, 2007]), lysine and tyrosine (cobalamin methyltransferase [Frank et al., 2007]), arginine and glutamate (DNA methyltransferase M.HhaI [Youngblood et al., 2007]), and histidine (M.EcoP151 DNA methyltransferase [Jois et al., 2008]).

The starting point for the catalytic reaction is formation of the Michaelis complex, in which both SAM and the DMVA acceptor substrate are bound to the enzyme. The amino moiety that accepts the methyl group from SAM would be expected to exist in the NH_3^+ form at neutral pH, thereby requiring deprotonation in order for it to act as an acceptor. In our MtfA-DMVA model, His228 and Arg230 are close to the N1 amide nitrogen of the substrate (Figure 3D), but only the H228A mutation has a drastic effect on enzyme activity (Table 2). The modeled distance between NE^{His228} and the N1 nitrogen of the substrate of 4.2 Å is somewhat larger than the H-bonding distance required for His228 to act as a general base. This may be because the imposed distance restrains attempted to simultaneously satisfy the spatial requirements of two distinct, subsequent mechanistic steps (i.e., proton abstraction and nucleophilic attack). However, the substrate N1 atom might have to move between the proton abstraction and methyl transfer steps. Thus, abstraction of the proton by the His228 base would require not only a rotation of the resulting lone electron-pair away from the base and toward the SAM methyl group but also a subsequent translation of the amino group in order to alleviate an electrostatic repulsion between its hydrogen atoms and the protonated His228. Indeed,

a distance of 8.5 Å between the SAM methyl and His228 imidazole in the crystal structure suggests that the substrate's receptor group oscillates between the two during catalysis. The Tyr32 and Glu144 residues are further away from DMVA and interact with SAM. The attenuated effect of their mutation on activity (~5-fold; Table 2) may therefore reflect their contribution to correct binding and orientation of the cofactor for methyl transfer. Tyr32 could, however, also participate through H bond interaction to optimally position the methyl group with respect to the acceptor for direct S_N2 transfer. This would be comparable to the role of Tyr221 in guanidinoacetate methyltransferase for which the Y221F mutation increased the K_M for SAM by 500-fold (Komoto et al., 2004) and a similar Tyr-to-Phe mutation in glycine *N*-methyltransferase that increased the K_M for the glycine substrate (Takata et al., 2003).

Overall, the precise, in-line positioning of the nucleophilic substrate amino moiety with respect to the *S*-methyl bond of the cofactor are requirements for effective methyl transfer and probably represent a significant contribution to reducing the activation energy barrier for catalysis by these enzymes. The ground state average S^{SAM}-C^{SAM}-$N1^{DMVA}$ atomic configuration obtained after 3 ns of MD simulation forms an angle of 150° with a distance between the nucleophilic N1 nitrogen of DMVA and the electrophilic methyl carbon of SAM of 4.2 Å (Figure 3D). This configuration is consistent with that obtained by hybrid quantum mechanics and molecular mechanics calculations and MD simulations for a similar methyl transfer reaction, from SAM to a target lysine amino group, catalyzed by lysine methyltransferases (Zhang and Bruice, 2008).

Most kinetic mechanisms for MTases indicate that the SAM cofactor binds first, followed by the acceptor, with the methylated product leaving first from the enzyme (Lakowski and Frankel, 2008). While this has not been investigated for MtfA, the crystal structure with modeled DMVA substrate is consistent with this proposal. Indeed, inspection of the molecular surface shows that SAM is largely buried when the DMVA substrate is positioned within the active site cleft.

SIGNIFICANCE

GPAs are an important class of anti-infective agents with activity against Gram-positive bacterial pathogens that are challenged by the emergence of resistance. The complex chemical structures of these antibiotics preclude total synthesis of analogs as second and third generation GPAs, which means that semisynthesis using known natural product scaffolds remains the key route to increased chemical diversity of this class of antibiotics. We have shown that the MTase MtfA can expand the chemical diversity of teicoplanin-like GPAs by additional methylation of the peptide scaffold in vitro and in vivo. The 3D structure of MtfA and molecular modeling shows that the antibiotic substrate binds in a cleft located at the dimer interface, created by association of the monomers through wing-like extensions. Since second generation GPAs already in clinical trials have been shown to overcome GPA resistance even with relatively minor modification, enzyme-catalyzed methyl transfer can now be explored as another approach to generate methylated GPA derivatives.

EXPERIMENTAL PROCEDURES

Cloning *mtfA* from *A. orientalis* and Integration into *S. toyocaensis*

The *mtfA* gene from the chloroeremomycin producer *A. orientalis* (van Wageningen et al., 1998) was amplified using the following oligonucleotide primers: 5′-AGCTCTAGA*CAT**ATG***AGCAATCAACTGGAGCGTGG-3′ and 5′-AGC*AAG CTT*TCTAGATCTGGCTTGCCGCGCTCA**TCA**C-3′, in which the putative start and stop codons (bold), the XbaI and BglII sites (underlined), and the NdeI and HindIII sites (italicized) are indicated. There is also a second XbaI site on the reverse primer that overlaps the BglII site. Genomic DNA was prepared from *A. orientalis* using the procedure previously described for *S. toyocaensis* (Neu et al., 2002; Lamb et al., 2006). PCR conditions were as follows: 3 min at 94°C, 30 cycles of 1 min at 94°C, 1 min at 57.5°C, and 1 min at 72°C, and 10 min at 72°C with 1 U BIOTOOLS DNA polymerase (Intersciences Inc.), 5% DMSO, and 3.5 mM exogenous $MgCl_2$.

The 850 bp PCR-amplified product was gel purified and ligated into the pCRII-TOPO (TOPO-TA) vector (Invitrogen Canada Inc.), followed by transformation into *E. coli* TOP10 competent cells. Isolation of the DNA from the transformants was analyzed by restriction digests, and constructs with an 850 bp insert were further confirmed by sequencing. This initial construct was designated *cmt*/TOPO-TA (for chloroeremomycin methyltransferase) but it was later discovered that the gene had been previously cloned (i.e., *mtfA*) (O'Brien et al., 2000). Henceforth, the designation of *mtfA* will be used.

Due to an overlapping XbaI-BglII site on the *mtfA* reverse primer, the *mtfA*/TOPO-TA vector was first digested with BglII and then with XbaI. The resulting 850 bp fragment (XbaI-BglII digested) was ligated into XbaI-BglII-digested pIJ8600, followed by transformation into *E. coli* TOP10. Isolated plasmid DNA from the transformants was analyzed by four separate restriction digests.

Transformation of *mtfA*/pIJ8600 into pUZ8002/ET12567 facilitated its subsequent conjugation and integration into both wild-type *S. toyocaensis* and *S. toyocaensis ΔstaL*::*aac(3)IV*. Confirmation of the two strains, *S. toyocaensis* ΦC31::*mtfA*/pIJ8600 and *S. toyocaensis ΔstaL*::*aac(3)IV* ΦC31::*mtfA*/pIJ8600, was primarily based on phenotype (i.e., thiostrepton [Tsr] resistance at 10 μg/mL) and by the amplification of *mtfA* via colony PCR. Tsr-resistant colonies of each *S. toyocaensis mtfA* integration strain were picked from Bennett's agar plates, resuspended in 100 μl of water, incubated in a boiling water bath for 10 min, and then used as template DNA (1 and 10 μl) for amplification of *mtfA* using the PCR conditions previously described. Genomic DNA from *A. orientalis* was used as a positive control and genomic DNA from *S. toyocaensis* and *S. toyocaensis ΔstaL*::*aac(3)IV* were used as negative controls.

The expression of *mtfA* in the two *S. toyocaensis mtfA* integration strains was confirmed by performing an RNA extraction on ~100 μg of the cell pellets using the GenElute mammalian total RNA kit (Sigma-Aldrich Canada), followed by DNaseI treatment using the TURBO DNA-free kit (Ambion Inc.), and then amplification of *mtfA* was carried out using the One Step RT-PCR kit (QIAGEN). The *S. toyocaensis mtfA* integration strains were grown for 3 days in 25 ml tryptone-soya broth CM0129 (TSB) (Oxoid Ltd) with and without Tsr (i.e., induced and noninduced, respectively) and the negative controls *S. toyocaensis* and *S. toyocaensis ΔstaL*::*aac(3)IV* were grown in 25 ml TSB for 3 days. Cultures were centrifuged (3000 rpm for 10 min at 4°C) and the cell pellets were washed in 25 ml of 10 mM Tris (pH 7.2) and stored at −80°C until analyzed as described.

Antibiotic Production and Analysis

The two *S. toyocaensis mtfA* integration strains were cultivated in Streptomyces Vegetative Medium plus Tsr for 3 days, followed by subculturing 500 μl into 50 ml Streptomyces Antibiotic Medium plus Tsr in a 250 ml Erlenmeyer flask. Culture supernatants and antibiotic extracts were prepared as previously described (Lamb et al., 2006). Extracts were subjected to analysis by disk-agar diffusion (20 μl), RP-HLPC (20 μl), and LC/ESI-MS (50 μl) using the conditions previously reported (Lamb et al., 2006). Note that extracts were made up to 100 μl in 15 mM HEPES (pH 7.5) prior to analysis by RP-HPLC.

Construction of the *mtfA* Expression Vector and Site-Directed Mutagenesis of *mtfA*

An 850 bp fragment (NdeI-BglII digested) was subcloned from *mtfA*/TOPO-TA and was ligated into NdeI-BamHI-digested pET28a. Subsequent transformation into *E. coli* BL21(DE3), followed by plasmid DNA isolation and restriction digest analyses, confirmed the construction of the expression vector *mtfA*/pET28a.

The *mtfA*/pET28a construct was used as a template for site-directed mutagenesis to construct four mutants with single amino acid alterations (Y32F, E144A, H228A, and R230A). The protocol used was based on the QuikChange site-directed mutagenesis kit (Stratagene). The primers used for site-directed mutagenesis are shown in Table S1. The PCR conditions used in a 50 μl reaction were ~55 ng *mtfA*/pET28a, 125 ng of forward and reverse primers, 0.8 mM dNTPs, 5% (v/v) dimethylsulfoxide, 4 mM $MgCl_2$, and 2.5 U Stratagene PFU Ultra. The PCR program used was 95°C for 3 min; 95°C for 1 min, annealing temperature (see Table S1) for 1 min, and 68°C for 7 min; and 68°C for 15 min. The PCR products were treated with 10 U of *DpnI* for 1 hr at 37°C and transformed into *E. coli* TOP10 cells using electroporation. Products were analyzed by complete gene sequencing to ensure the desired mutations were introduced.

Purification of MtfA and Mutant Proteins

Wild-type and mutant *mtfA* genes were expressed with an N-terminal His_6 tag. For the production of selenomethionine (SeMet)-labeled protein the *E. coli* methionine auxotroph strain DL41(DE3) was transformed with the plasmid (Hendrickson et al., 1990). An overnight culture of transformed *E. coli* BL21(DE3) or DL41(DE3) was used to inoculate 1l 2YT medium (or LeMaster medium with 25 mg/l L-SeMet) containing 50 μg/ml kanamycin and grown at 37°C until OD_{600} reached 0.6. Protein expression was induced with 100 μM isopropyl 1-thio-β-*D*-galactopyranoside followed by 16–20 hr incubation at 16°C. The cells were harvested by centrifugation (4000 × g, 4°C, 25 min), resuspended in 40 ml of lysis buffer (50 mM HEPES [pH 7.5], 0.5 M NaCl, 20 mM imidazole [pH 8], and 1 mM dithiothreitol [DTT]), and lysed by sonication (10 × 12 s, with 20 s between bursts). After ultracentrifugation (100,000 × g, 45 min, 4°C) the protein supernatant was loaded onto 2 ml (bed volume) of Ni-NTA agarose resin (QIAGEN) equilibrated with lysis buffer. The column was washed with 40 ml of buffer A (50 mM HEPES [pH 7.5], 1.0 M NaCl, 20 mM imidazole, and 1 mM DTT) and 40 ml of buffer B (50 mM HEPES [pH 7.5], 0.4 M NaCl, 30 mM imidazole, and 1 mM DTT). His_6-MtfA was eluted with buffer B supplemented to 200 mM imidazole and concentrated by ultrafiltration to 15 mg/ml with concomitant buffer exchange to 20 mM HEPES [pH 7.5], 20 mM NaCl, and 5 mM DTT. Dynamic light scattering measurements were performed at room temperature using a DynaPro plate reader (Wyatt Technologies). SeMet-labeled protein was purified following the same protocol.

Mutant and wild-type His_6-MtfA proteins were analyzed by circular dichroism. Protein concentrations were adjusted to 0.19 mg/ml in 50 mM NaH_2PO_4 buffer [pH 8.0] with 5% (v/v) glycerol. 250 μl of protein was added to a 1 mm Hellma quartz cell (minimum wavelength of 175 nm) at 25°C and sample measurements were taken every 1 nm at an average time of 3 s in a 195–260 nm spectrum using an AVIV 410 Circular Dichroism Spectrometer (Aviv Biomedical Inc).

Substrate Specificity of MftA

Desulfo-A47934, A47934, and teicoplanin were tested as substrates for His_6-MtfA in reactions (50 μl) typically containing 2 mM SAM, 1 mg/ml BSA, 10% DMSO, 10 μM His_6-MtfA (3 μg), 500 μM substrate, and 75 mM Tris-HCl [pH 8.0]. Control reactions were set up with no His_6-MtfA added. All reactions were incubated at 30°C for specific time points, stopped by adding an equal volume of cold methanol, incubated at −20°C for 20 min, and centrifuged for 5 min at 13,000 rpm. Subsequent analysis of the supernatant (50 μl) was performed using LC/ESI-MS. Preliminary substrate reactions were set up in a similar manner but contained 1 μM His_6-MtfA (0.3 μg) and 250 μM desulfo-A47934, A47934 or teicoplanin as substrates. These reactions were incubated for 18 hr and were analyzed by RP-HPLC (100 μl) and LC/ESI-MS (50 μl). The extract (10 μl) from the *S. toyocaensis ΔstaL*::*aac(3)IV* ΦC31::*mtfA*/pIJ8600 strain was used in place of substrate in methylation reactions with 1 μM His_6-MtfA (0.3 μg). The reaction was incubated for 16 hr, stopped, and analyzed via RP-HPLC. All RP-HPLC and LC/ESI-MS experiments described in this section used the previously reported conditions for each substrate (Lamb et al., 2006).

Determination of MftA Enzyme Activity

The enzyme activity of His_6-MtfA was analyzed by LC/ESI-MS. Each reaction was performed in triplicate under initial rate conditions and consisted of 0.5 mM SAM, 50 μM desulfo-A47934, and 3 μg of His_6-MtfA in 50 mM HEPES buffer (pH 7.5) in a final volume of 50–100 μl incubated for 1–24 hr at 30°C and the reactions stopped by adding 1% (v/v) trifluoroacetic acid. Reaction products were analyzed by LC/ESI-MS using a ZORBAX Eclipse XD8-C8 column with solvent A (0.05% formic acid in water) and solvent B (acetonitrile with 0.05% formic acid). Samples were analyzed both for UV absorbance (220–280 nm) and by mass using an Applied Biosystems QTRAP LC/ESI-MS/MS instrument.

The progress of enzymatic reactions was followed by RP-HPLC by measuring the area under the curve of peaks at 280 nm and comparing to a standard curve of desulfo-A47934 concentration. Mutants of His_6-MtfA were tested and compared to wild-type His_6-MtfA. Reactions were performed in triplicate and error was calculated by determining the standard deviation between the samples.

Crystallization of MtfA

Initial crystallization conditions were determined by the hanging drop vapor diffusion method at 21°C using in-house screens. The best crystals were obtained by equilibrating 1 μl of protein mixed with 1 μl of reservoir solution (0.1 M MES [pH 6.5] and 18% [w/v] PEG monomethyl ether 5000) over 0.5 ml of reservoir solution at 21°C. Crystals belong to space group *C*2 with unit cell dimensions $a = 127.4$, $b = 71.7$, $c = 75.2$ Å, and $\beta = 103.0°$ and contain two molecules in the asymmetric unit with a $V_m = 2.54$ $Å^3Da^{-1}$. SeMet-labeled protein crystallized under the same conditions. For data collection, crystals were transferred to a solution containing reservoir solution supplemented with 16% (v/v) ethylene glycol and flash cooled in a nitrogen stream at 100 K (Oxford Cryosystems).

Complexes of MtfA with SAM (Sigma-Aldrich Canada) or SAH (Fluka) were obtained by soaking apo crystals in the reservoir solution supplemented with 20 mM SAM or 10 mM SAH. The complex with sinefungin (Calbiochem) was obtained by soaking crystals in reservoir solution supplemented with 2 mM sinefungin.

X-Ray Data Collection, Structure Solution, and Refinement

Diffraction data from a SeMet-labeled MtfA crystal were collected at the Se anomalous peak (Table 3) with a Quantum-4 CCD detector (Area Detector Systems Corp.) at beamline X8C at the National Synchrotron Light Source, Brookhaven National Laboratory. Data integration and scaling was performed with HKL2000 (Otwinowski and Minor, 1997). The structure was determined by single-wavelength anomalous dispersion at the Se peak energy and refined using 2.0 Å resolution data. The Se substructure was solved using SHELXD/E (Schneider and Sheldrick, 2002), 55% of the model was built into the 2.0 Å map using ARP/wARP (Perrakis et al., 1999), and the remainder modeled with COOT (Emsley and Cowtan, 2004). The model was refined using REFMAC5 (Murshudov et al., 1999). The translation-libration-screw temperature factor model was used near the end of refinement and the final R_{work} and R_{free} are 0.238 and 0.271, respectively.

A data set from crystals of the MtfA-SAM complex was collected to 2.10 Å resolution at the Lilly Research Laboratory Collaborative Access Team (LRL-CAT) beamline, Advanced Photon Source, Argonne National Laboratory. The structure was solved by molecular replacement (MOLREP [Vagin and Teplyakov, 1997]) using apo-MtfA as a search model and refined to a R_{work} and R_{free} of 0.216 and 0.245, respectively. Diffraction data from MtfA-SAH crystals were collected to 2.95 Å resolution on an RAXIS-HTC detector mounted on a Rigaku 007 microfocus rotating anode and the structure refined to a R_{work} and R_{free} of 0.209 and 0.259, respectively. The MtfA-sinefungin complex was refined against data collected to 2.18 Å at LRL-CAT (R_{work} = 0.226 and R_{free} = 0.253). Final data collection, refinement statistics, and Protein Data Bank accession codes are shown in Table 3.

Molecular Docking of DMVA Substrate to MtfA-SAM Enzyme-Cofactor Complex

For docking calculations, SYBYL (Tripos, Inc.) was used to reconstruct the missing side chains of the MtfA dimer, add hydrogen atoms corresponding to neutral pH protonation state, and block chain termini with acetyl and methylamino groups. The MtfA-SAM complex was conjugate gradient energy minimized with an 8 Å nonbonded cutoff and a distance-dependent dielectric ($4R_{ij}$) using the AMBER force field and partial charges (Lee and Duan, 2004) for the

Table 3. X-Ray Data Collection and Refinement Statistics

Data Set	SeMet (SAD)	MtfA-SAM	MtfA-SAH	MtfA-Sinefungin
Space Group	*C*2			
a (Å)	127.4	126.9	126.5	126.6
b (Å)	71.7	72.3	72.5	71.9
c (Å)	75.2	75.3	75.2	75.1
β (°)	103.0	103.9	104.2	103.8
Wavelength (Å)	0.9800	0.9798	1.5418	0.9798
Resolution (Å)	50–2.0 (2.07–2.0)	50–2.10 (2.18–2.10)	50–2.96 (3.07–2.96)	50–2.18 (2.26–2.18)
Observed *hkl*	213,120	122,177	50,950	109,760
Unique *hkl*	85,936 (unmerged)	35,055	13,628	31,659
Redundancy	2.5 (2.2)	3.5 (2.6)	3.7 (3.7)	3.5 (2.4)
Completeness (%)	97.4 (84.6)	90.8 (60.9)	97.5 (96.3)	92.2 (64.1)
R_{sym} [a]	0.046 (0.315)	0.040 (0.276)	0.112 (0.500)	0.043 (0.290)
I/σ (I)	19.9 (2.5)	21.6 (2.7)	10.3 (2.5)	19.4 (2.6)
Wilson B ($Å^2$)	35.2	38.3	76.2	41.9
R_{work} [b] (*#hkl*)	0.238 (42,094)	0.216 (33,246)	0.209 (12,944)	0.226 (30,031)
R_{free} (*#hkl*)	0.271 (2,239)	0.245 (1,783)	0.259 (684)	0.253 (1,589)
B factors (#atoms)				
Protein	41.9 (3,432)	48.1 (3,608)	50.8 (3,709)	50.6 (3,634)
Solvent	38.9 (143)	48.0 (144)	40.0 (9)	44.4 (124)
Ligands	–	51.0 (54)	50.2 (45)	48.8 (54)
Ramachandran				
Allowed (%)	99.7	98.7	98.3	98.7
Generous (%)	0.3	0.8	1.2	1.0
Disallowed (%)	0	0.5	0.5	0.3
Rmsd				
Bonds (Å)	0.007	0.011	0.012	0.011
Angles (°)	1.05	1.30	1.49	1.44
PDB code	3G2M	3G2O	3G2P	3G2Q

[a] $R_{sym} = (\Sigma|I_{obs} - I_{avg}|)/\Sigma I_{avg}$.
[b] $R_{work} = (\Sigma|F_{obs} - F_{calc}|)/\Sigma F_{obs}$.

protein dimer and the GAFF force field (Wang et al., 2004) and AM1-BCC partial charges (Jakalian et al., 2002) for the SAM cofactor. The starting structure of DMVA was taken from the crystal structure of the GtfA-vancomycin complex (PDB code 1PN3 [Mulichak et al., 2003]), followed by *O*-deglycosylation, *N*1-demethylation, addition of hydrogen atoms, and assignment of AM1-BCC partial charges for a protonation state corresponding to a neutral N1 amino group. While minor conformational changes of the antibiotic core exist between the free and various bound vancomycin structures available, these changes are within the conformational space sampled by MD; thus making any of those structures appropriate for the modeling procedure adopted here.

We used in-house exhaustive docking software for generating and ranking feasible binding modes of DMVA to the MtfA-SAM complex. Ligand poses were scored with a binding affinity scoring function calibrated against known protein-ligand complexes (Wang et al., 2005) that included van der Waals, Coulombic, hydrogen bonding, surface complementarily, and polar desolvation surface area terms. A rigid docking was used in which single-conformation representations of the MtfA-SAM target and the DMVA ligand were taken from their respective crystal structures. One binding pose was selected based on a high binding affinity score and the reactive distance between the nucleophilic amine N1 nitrogen atom of DMVA and the reactive *S*-methyl carbon of SAM.

This MtfA-SAM-DMVA complex was sampled by a 3 ns MD simulation. The AMBER 9 suite of programs (Case et al., 2005) was used for MD simulation and trajectory analysis. The complex was solvated in a truncated octahedron TIP3P water box (Jorgensen et al., 1983) and the electroneutrality of the system was achieved by the addition of 17 Na^+ counterions. Applying harmonic restraints with force constants of 20 kcal mol^{-1} $Å^{-2}$ to all solute atoms, the system was energy minimized, followed by heating from 100 to 300 K over 25 ps in the canonical ensemble (NVT) and by equilibrating to adjust the solvent density under 1 atmospheric pressure over 25 ps in the isothermal-isobaric ensemble (NPT) simulation. The harmonic restraints were then gradually reduced to zero with four rounds of 25 ps simulations. The nucleophilic N1 amine nitrogen atom of DMVA was restrained to be within 3.0–4.5 Å from the reactive *S*-methyl carbon of SAM and from the $NE1^{His228}$ atom. The ends encompassing a disordered loop between residues Ala36 and Asp48 were also restrained to within 18.0–19.5 Å. After an additional 25 ps simulation, a 3 ns production NPT run was performed with snapshots collected every 1 ps, using a 2 fs time step and 9 Å nonbonded cutoff. The Particle Mesh Ewald method (Darden et al., 1993) was used to treat long-range electrostatic interactions, and bond lengths involving bonds to hydrogen atoms were constrained by SHAKE (Ryckaert et al., 1977). The final complex structure was obtained by coordinate averaging over the last 1 ns of MD trajectory, followed by 1000 steps of energy minimization without any restraints.

ACCESSION NUMBERS

Coordinates of MtfA, MtfA-SAM, MtfA-SAH, and MtfA-sinefungin complexes have been deposited to Protein Data Bank with accession codes 3G2M, 3G2O, 3G2P, and 3G2Q, respectively.

SUPPLEMENTAL DATA

Supplemental Data contain two figures and one table and can be found with this article online at http://www.cell.com/chemistry-biology/supplemental/S1074-5521(09)00073-8.

ACKNOWLEDGMENTS

This research was supported in part by grants from the Canadian Institutes of Health Research (MT-14981 to G.D.W. and GSP-48370 to M.C.) and a Canada Research Chair (to G.D.W.). X-ray diffraction data for this study were measured at beamlines X8C and X29 of the National Synchrotron Light Source (NSLS), Brookhaven National Laboratory, and Lilly Research Laboratory Collaborative Access Team (LRL-CAT) at the Advanced Photon Source, Argonne National Laboratory. Financial support for the NSLS comes principally from the Office of Biological and Environmental Research and of Basic Energy Sciences of the U.S. Department of Energy and the National Center for Research Resources of the National Institutes of Health. Use of the Advanced Photon Source at Argonne National Laboratory was supported by the U.S. Department of Energy, Office of Basic Energy Sciences, under contract number DE-AC02-06CH11357. Use of the LRL-CAT beamline facilities at Sector 31 of the Advanced Photon Source was provided by Eli Lilly and Company, who operates the facility. This is National Research Council Canada publication 49594.

Received: November 16, 2008
Revised: February 6, 2009
Accepted: February 16, 2009
Published: April 23, 2009

REFERENCES

Attwood, R.J., and LaPlante, K.L. (2007). Telavancin: a novel lipoglycopeptide antimicrobial agent. Am. J. Health Syst. Pharm. *64*, 2335–2348.

Banik, J.J., and Brady, S.F. (2008). Cloning and characterization of new glycopeptide gene clusters found in an environmental DNA megalibrary. Proc. Natl. Acad. Sci. USA *105*, 17273–17277.

Billeter, M., Zervos, M.J., Chen, A.Y., Dalovisio, J.R., and Kurukularatne, C. (2008). Dalbavancin: a novel once-weekly lipoglycopeptide antibiotic. Clin. Infect. Dis. *46*, 577–583.

Case, D.A., Cheatham, T.E., III, Darden, T., Gohlke, H., Luo, R., Merz, K.M., Jr., Onufriev, A., Simmerling, C., Wang, B., and Woods, R.J. (2005). The Amber biomolecular simulation programs. J. Comput. Chem. *26*, 1668–1688.

Darden, T., York, D., and Pedersen, L. (1993). Particle mesh Ewald: an N log(N) method for Ewald sums in large systems. J. Chem. Phys. *98*, 10089–10092.

Donadio, S., Sosio, M., Stegmann, E., Weber, T., and Wohlleben, W. (2005). Comparative analysis and insights into the evolution of gene clusters for glycopeptide antibiotic biosynthesis. Mol. Genet. Genomics *274*, 40–50.

Emsley, P., and Cowtan, K. (2004). Coot: model-building tools for molecular graphics. Acta Crystallogr. D Biol. Crystallogr. *60*, 2126–2132.

Frank, S., Deery, E., Brindley, A.A., Leech, H.K., Lawrence, A., Heathcote, P., Schubert, H.L., Brocklehurst, K., Rigby, S.E.J., Warren, M.J., and Pickersgill, R.W. (2007). Elucidation of substrate specificity in the cobalamin (vitamin B12) biosynthetic methyltransferases. Structure and function of the C20 methyltransferase (CbiL) from *Methanobacter thermoautotrophicus*. J. Biol. Chem. *282*, 23957–23969.

Guo, H.B., and Guo, H. (2007). Mechanism of histone methylation catalyzed by protein lysine methyltransferase SET7/9 and origin of product specificity. Proc. Natl. Acad. Sci. USA *104*, 8797–8802.

Hendrickson, W.A., Horton, J.R., and LeMaster, D.M. (1990). Selenomethionyl proteins produced for analysis by multiwavelength anomalous diffraction (MAD): a vehicle for direct determination of three-dimensional structure. EMBO J. *9*, 1665–1672.

Jakalian, A., Jack, D.B., and Bayly, C.I. (2002). Fast, efficient generation of high-quality atomic charges. AM1-BCC model: II. Parameterization and validation. J. Comput. Chem. *23*, 1623–1641.

Jois, P.S., Madhu, N., and Rao, D.N. (2008). Role of histidine residues in EcoP15I DNA methyltransferase activity as probed by chemical modification and site-directed mutagenesis. Biochem. J. *410*, 543–553.

Jorgensen, W.L., Chandrasekhar, J., Madura, J.D., Impey, R.W., and Klein, M.L. (1983). Comparison of simple potential functions for simulating liquid water. J. Chem. Phys. *79*, 926–935.

Kahne, D., Leimkuhler, C., Lu, W., and Walsh, C. (2005). Glycopeptide and lipoglycopeptide antibiotics. Chem. Rev. *105*, 425–448.

Komoto, J., Yamada, T., Takata, Y., Konishi, K., Ogawa, H., Gomi, T., Fujioka, M., and Takusagawa, F. (2004). Catalytic mechanism of guanidinoacetate methyltransferase: crystal structures of guanidinoacetate methyltransferase ternary complexes. Biochemistry *43*, 14385–14394.

Lakowski, T.M., and Frankel, A. (2008). A kinetic study of human protein arginine N-methyltransferase 6 reveals a distributive mechanism. J. Biol. Chem. *283*, 10015–10025.

Lamb, S.S., Patel, T., Koteva, K.P., and Wright, G.D. (2006). Biosynthesis of sulfated glycopeptide antibiotics by using the sulfotransferase StaL. Chem. Biol. *13*, 171–181.

Lee, M.C., and Duan, Y. (2004). Distinguish protein decoys by using a scoring function based on a new AMBER force field, short molecular dynamics simulations, and the generalized born solvent model. Proteins *55*, 620–634.

Losey, H.C., Jiang, J., Biggins, J.B., Oberthur, M., Ye, X.Y., Dong, S.D., Kahne, D., Thorson, J.S., and Walsh, C.T. (2002). Incorporation of glucose analogs by GtfE and GtfD from the vancomycin biosynthetic pathway to generate variant glycopeptides. Chem. Biol. *9*, 1305–1314.

Mulichak, A.M., Losey, H.C., Lu, W., Wawrzak, Z., Walsh, C.T., and Garavito, R.M. (2003). Structure of the TDP-epi-vancosaminyltransferase GtfA from the chloroeremomycin biosynthetic pathway. Proc. Natl. Acad. Sci. USA *100*, 9238–9243.

Mulichak, A.M., Lu, W., Losey, H.C., Walsh, C.T., and Garavito, R.M. (2004). Crystal structure of vancosaminyltransferase GtfD from the vancomycin biosynthetic pathway: interactions with acceptor and nucleotide ligands. Biochemistry *43*, 5170–5180.

Murray, B.E. (2000). Vancomycin-resistant enterococcal infections. N. Engl. J. Med. *342*, 710–721.

Murshudov, G.N., Vagin, A.A., Lebedev, A., Wilson, K.S., and Dodson, E.J. (1999). Efficient anisotropic refinement of macromolecular structures using FFT. Acta Crystallogr. D Biol. Crystallogr. *55*, 247–255.

Neu, J.M., MacMillan, S.V., Nodwell, J.R., and Wright, G.D. (2002). StoPK-1, a serine/threonine protein kinase from the glycopeptide antibiotic producer *Streptomyces toyocaensis* NRRL 15009, affects oxidative stress response. Mol. Microbiol. *44*, 417–430.

O'Brien, D.P., Kirkpatrick, P.N., O'Brien, S.W., Staroske, T., Richardson, T.I., Evans, D.A., Hopkins, A., Spencer, J.B., and Williams, D.H. (2000). Expression and assay of an N-methyltransferase involved in the biosynthesis of a vancomycin group antibiotic. Chem. Commun. (Camb.) *1*, 103–104.

Otwinowski, Z., and Minor, W. (1997). Processing of X-ray diffraction data collected in oscillation mode. Methods Enzymol. *276*, 307–326.

Perrakis, A., Morris, R., and Lamzin, V.S. (1999). Automated protein model building combined with iterative structure refinement. Nat. Struct. Biol. *6*, 458–463.

Poulakou, G., and Giamarellou, H. (2008). Oritavancin: a new promising agent in the treatment of infections due to Gram-positive pathogens. Expert Opin. Investig. Drugs *17*, 225–243.

Pugh, C.S., Borchardt, R.T., and Stone, H.O. (1978). Sinefungin, a potent inhibitor of virion mRNA(guanine-7-)-methyltransferase, mRNA(nucleoside-2′-)-methyltransferase, and viral multiplication. J. Biol. Chem. *253*, 4075–4077.

Recktenwald, J., Shawky, R., Puk, O., Pfennig, F., Keller, U., Wohlleben, W., and Pelzer, S. (2002). Nonribosomal biosynthesis of vancomycin-type antibiotics: a heptapeptide backbone and eight peptide synthetase modules. Microbiology *148*, 1105–1118.

Rodriguez, M.J., Snyder, N.J., Zweifel, M.J., Wilkie, S.C., Stack, D.R., Cooper, R.D., Nicas, T.I., Mullen, D.L., Butler, T.F., and Thompson, R.C. (1998). Novel glycopeptide antibiotics: N-alkylated derivatives active against vancomycin-resistant enterococci. J. Antibiot. (Tokyo) *51*, 560–569.

Ryckaert, J.P., Ciccotti, G., and Berendsen, H.J.C. (1977). Numerical integration of the cartesian equations of motion of a system with constraints: molecular dynamics of n-alkanes. J. Comp. Phys. *23*, 327–341.

Schneider, T.R., and Sheldrick, G.M. (2002). Substructure solution with SHELXD. Acta Crystallogr. D Biol. Crystallogr. *58*, 1772–1779.

Schubert, H.L., Blumenthal, R.M., and Cheng, X. (2003). Many paths to methyltransfer: a chronicle of convergence. Trends Biochem. Sci. *28*, 329–335.

Shi, R., Lamb, S.S., Bhat, S., Sulea, T., Wright, G.D., Matte, A., and Cygler, M. (2007). Crystal structure of StaL, a glycopeptide antibiotic sulfotransferase from *Streptomyces toyocaensis*. J. Biol. Chem. *282*, 13073–13086.

Sosio, M., Stinchi, S., Beltrametti, F., Lazzarini, A., and Donadio, S. (2003). The gene cluster for the biosynthesis of the glycopeptide antibiotic A40926 by *Nonomuraea* species. Chem. Biol. *10*, 541–549.

Takata, Y., Huang, Y., Komoto, J., Yamada, T., Konishi, K., Ogawa, H., Gomi, T., Fujioka, M., and Takusagawa, F. (2003). Catalytic mechanism of glycine N-methyltransferase. Biochemistry *42*, 8394–8402.

Vagin, A., and Teplyakov, A. (1997). MOLREP: an automated program for molecular replacement. J. Appl. Crystallogr. *30*, 1022–1025.

Van Bambeke, F., Van, L.Y., Courvalin, P., and Tulkens, P.M. (2004). Glycopeptide antibiotics: from conventional molecules to new derivatives. Drugs *64*, 913–936.

van Wageningen, A.M., Kirkpatrick, P.N., Williams, D.H., Harris, B.R., Kershaw, J.K., Lennard, N.J., Jones, M., Jones, S.J., and Solenberg, P.J. (1998). Sequencing and analysis of genes involved in the biosynthesis of a vancomycin group antibiotic. Chem. Biol. *5*, 155–162.

Wang, J., Wolf, R.M., Caldwell, J.W., Kollman, P.A., and Case, D.A. (2004). Development and testing of a general amber force field. J. Comput. Chem. *25*, 1157–1174.

Wang, R., Fang, X., Lu, Y., Yang, C.Y., and Wang, S. (2005). The PDBbind database: methodologies and updates. J. Med. Chem. *48*, 4111–4119.

Youngblood, B., Shieh, F.K., Buller, F., Bullock, T., and Reich, N.O. (2007). S-adenosyl-L-methionine-dependent methyl transfer: observable precatalytic intermediates during DNA cytosine methylation. Biochemistry *46*, 8766–8775.

Zhang, X., and Bruice, T.C. (2008). Mechanism of product specificity of AdoMet methylation catalyzed by lysine methyltransferases: transcriptional factor p53 methylation by histone lysine methyltransferase SET7/9. Biochemistry *47*, 2743–2748.

